Fractal laser glints from the ocean surface

Joseph A. Shaw and James H. Churnside

National Oceanic and Atmospheric Administration Environmental Technology Laboratory, 325 Broadway, Boulder, Colorado 80303

Received July 8, 1996; revised manuscript received November 5, 1996; accepted December 11, 1996

Time series of laser glint counts from the ocean surface exhibit fractal behavior. Glint-count histogram widths do not follow Gaussian statistics, and histogram shapes are approximately log normal. Fractal dimensions for the statistically self-similar glint-count time series are found from the power spectra, which have an inverse power-law form. Glint counts in one spatial dimension from a linearly scanning laser and glint counts in two spatial dimensions from a laser glint imager behave similarly. In both sets of data, spectral density peaks exist at frequencies corresponding to swell and long wind waves. This implies that the glint-count process contains information related to long-wave modulation of surface roughness. © 1997 Optical Society of America [S0740-3232(97)01205-2]

Key words: fractals, self-similarity, statistical optics, ocean optics, sea-surface roughness.

1. INTRODUCTION

Fractals, as first formalized by Mandelbrot,[1] generally can be described as geometrical structures having similar characteristics over a range of scales. That is, a fractal process has no characteristic size (or time) scale. Instead, it is characterized by a fractal dimension, which describes how wiggly the structure is relative to its smooth Euclidian counterpart. Essentially, the fractal dimension replaces the geometric length, which approaches infinity for a fractal that consists of wiggles upon wiggles on increasingly small scales, with a number that instead quantifies the degree of irregularity of the wiggly surface. The fractal dimension can be related to the spectral exponent β of an inverse-frequency power spectrum that varies with frequency f according to $f^{-\beta}$ over some spectral range. The fractal dimension of such a process in E Euclidian dimensions is related directly to the log–log power-spectrum slope by[2,3]

$$D = E + \frac{3 - \beta}{2}. \tag{1}$$

Thus time series that have $E = 1$ produce a fractal dimension of 2.5 for random white noise ($\beta = 0$), 2.0 for a $1/f$ process ($\beta = 1$), and 1.5 for a Brownian process ($\beta = 2$). Note that we use $E = 1$ for all of our analysis because we are computing the fractal dimension of time-series plots that have one Euclidian dimension, regardless of whether the glint counts are from a linear scan with one Euclidian dimension or from an image with two Euclidian dimensions.

The recent literature refers to an impressively large and varied collection of fractals in nature,[1–15] including coastlines, clouds, snowflakes, galaxies, and ocean waves. Two approaches have been taken for studying the fractal characteristics of ocean-wave processes. The first approach is to calculate the fractal dimension of the attractor that describes the evolution of a dynamical process in phase space.[4–6] The second approach is to calculate a fractal dimension of the process itself.[7–12] We follow the second approach and calculate the fractal dimension of glint-count time series. These time series are related to sea-surface roughness and are shown to contain useful information regarding nonlinear wave–wave interactions. Others have applied similar fractal approaches to wave heights,[7,8] images of breaking-wave regions,[9–11] and time series of laser glints from the ocean surface.[12] These processes have different fractal dimensions and scale ranges because they depend on different physical processes.

We recently deployed two laser glint instruments in the Pacific Ocean to measure slope statistics[16] and related sea-surface parameters, including fractal dimension. One instrument was a linearly scanning laser glint meter, which counted glints (specular reflections of laser light back to the instrument) from the sea surface in 1° angular bins from nadir out to ±70°; the other instrument was a video-laser glint imager, which recorded images of the glint pattern from an array of diode lasers in an approximately 8.7° × 6.4° full-angle field of view. The scanning-laser data set provides an opportunity to confirm the fractal results obtained with a similar scanning-laser glint sensor by Zosimov and Naugolnykh[12]; the glint video data set provides further insight into the glint-count process and its fractal characteristics.

Zosimov and Naugolnykh[12] analyzed time series of laser glint counts from a ship in the tropical and subtropical Atlantic Ocean under steady trade winds (8–10 m s^{-1} wind speeds). With the ship steaming into the wind, they scanned a narrow He–Ne laser beam ±8.6° from nadir in the cross-wind direction, at a rate of 25 Hz, and collected a record of the number of glints counted per second over the entire angular range. The resultant glint-count time series, at scales longer than the wind-wave correlation length, maintained a similar variance when the sample duration and time-series duration both were increased by an order of magnitude. Therefore the process clearly did not conform to typical Gaussian or Poisson statistics, for which the variance is expected to decrease in proportion to the sample duration (analogous to averaging time). This apparent statistical self-

0740-3232/97/0501144-07$10.00

similarity was manifested further in the glint-count power spectrum, which had a well-defined $f^{-0.86}$ form between approximately 0.02 and 0.2 Hz. As has been pointed out by several authors,[2,3,13–15] an $f^{-\beta}$ power spectrum is inherently self-similar and is therefore a common indicator of a fractal process.

Zaslavskii and Sharkov[11] counted the average number of breaking waves in areas of various sizes, from the correlation length (40 m for their conditions) to about five or six times larger. Their results exhibited a power-law dependence on the spatial dimension of the area with an exponent of 0.5. Both of the processes investigated in Refs. 11 and 12 are related to large-scale variability of wind waves, and the similarity of their resultant spectral exponents is interesting. However, it is difficult to draw precise conclusions from this comparison because of the inexact correspondence of the processes, particularly because the data were plotted versus time in one case and versus spatial dimension in the other.

Our scanning-laser results reported here are sufficiently similar to those of Zosimov and Naugolnykh[12] to be considered validation of the generality of their results for large-scale surface-roughness variability. We find much larger influence of swell on the shape of our glint-count power spectra, most likely a result of larger swell in our experiment than theirs. The laser glint image data exhibit a nearly identical fractal dimension for large-scale variability (frequencies lower than the dominant wind wave). The data also demonstrate a similar fractal behavior, with smaller fractal dimension, for small-scale variability (frequencies higher than the dominant wind wave). Our large-scale variability spectral exponents for glint counts in one and two spatial dimensions are close to Zaslavskii and Sharkov's value of 0.5 but smaller than Zosimov and Naugolnykh's 0.86 result. Furthermore, the glint images produce nearly identical fractal results with either a pixel-counting or a blob-counting approach, which is further evidence of a fractal characteristic that is nearly independent of counting technique.

An additional result that becomes more apparent as the time-series duration increases is that for both instruments, the glint-count histograms are approximately log normal. The existence of a log-normal histogram is related to the glint-count process arising from a series of multiplicative, interdependent, sequential events, which in turn suggests a fractal, or self-similar, process. West,[13] West and Shlesinger,[14] and Montroll and Shlesinger[15] have discussed how the lognormal distribution is related to $1/f$ noise and hence arises in many fractal processes.

In the balance of this paper we first describe the instruments and experimental deployment and then present the results of a fractal analysis of the data. We conclude by summarizing our results and suggesting some future applications and extensions of this work.

2. EXPERIMENTAL TECHNIQUE

The data considered here are from two collocated instruments deployed as part of the Coastal Ocean Probing Experiment (COPE) near the Oregon coast during September 1995. One was a scanning-laser glint meter, the other a video-laser glint imager. Both instruments were suspended on a stabilized mount from a boom on the Scripps Institution of Oceanography FLoating Instrument Platform (FLIP). The instruments were deployed at the boom end, approximately 10 m upwind from the FLIP during the times considered here, with the optics aperture 5–6 m above the ocean surface. Wind speeds during these measurements ranged from 1 to 6 m s^{-1}, with both positive and negative atmospheric stability (which is proportional to the air–sea temperature difference). All the data considered here were collected during nighttime operation to minimize the background-light level.

The scanning-laser glint meter records the number of glints above a threshold value in 1° angular bins for nadir angles out to ±70°. However, for comparison with the previous work of Zosimov and Naugolnykh[12] we processed our data in a similar manner by forming time series of the total number of glints in ±10° from nadir and examining the behavior of the corresponding histograms and power spectra on various time scales. There may be some difference because our data are for along-wind scans, whereas Zosimov and Naugolnykh's were for cross-wind scans.

The video-laser glint imager records laser glint images at a rate of 30 frames per second on videotape. The system consists of a CCD camera, with no automatic gain control and high contrast, and an array of diode lasers that illuminates the ocean surface with nearly uniform irradiance within the 8.7° × 6.4° camera field of view. A 10-nm bandpass filter isolates the laser light radiated at a nominal wavelength of 832 nm. Both continuous and amplitude-modulated laser modes are available. In the first mode all four 30-mW lasers are on all the time, whereas in the second, the lasers are modulated so that successive video frames see full laser illumination followed by no laser illumination. This mode is useful for determining the impact of background light and provides a convenient way to choose a glint threshold in postprocessing of the video images. Typically we recorded a few minutes of modulated-laser video at the beginning of each tape and then recorded the balance of the tape with the lasers on continuously if the background light level was sufficiently low.

We used two different counting techniques for the fractal analysis of video glint counts. Both techniques used binary images, for which each pixel contained a 1 if its value exceeded the threshold or a 0 if that pixel value was lower than the threshold value. In the first case we counted the number of glint pixels in each video frame, and in the second case, we counted the number of blobs, or glint regions, in each frame. A blob is any grouping of glint pixels that are connected horizontally or vertically. From the time series of these pixel or blob counts, we analyzed the behavior of the corresponding histograms and power spectra under a variety of physical and temporal conditions.

The number of glints in any given sample is equivalent to an integral of the product of the surface curvature and the slope probability density function over the appropriate angular range. Thus the glint-count variability can be considered to be a measure of the surface-roughness

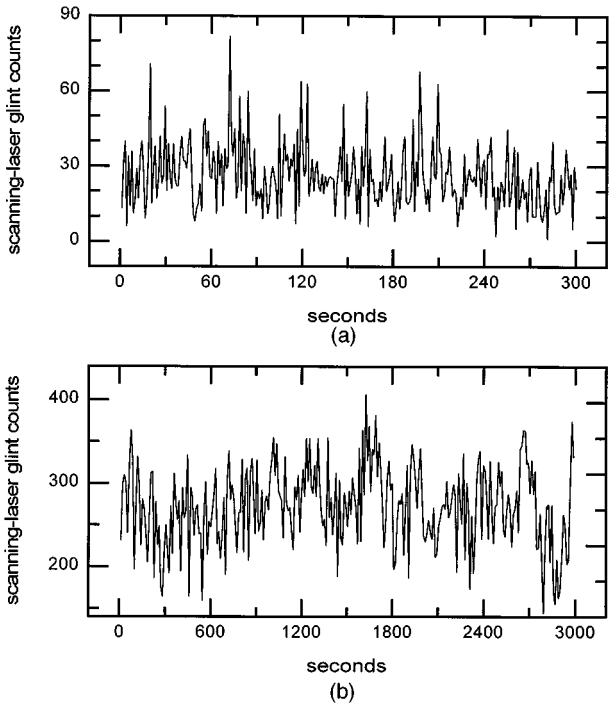

Fig. 1. Two time series from a 2-Hz scanning-laser glint meter of glint counts within ±10° of nadir. (a), 5 min of 10-s samples; (b), 50 min of 10-s samples.

variability and therefore highly related to both wave-slope and ripple (short-wave) variability.

3. EXPERIMENTAL RESULTS

We first examined the glint counts for low-frequency variability on scales longer than the wave correlation time. For well-developed waves the correlation time is approximately equal to the period of the dominant wind wave at wind speed U:

$$T = \frac{2\pi U}{g}, \tag{2}$$

with g representing the gravitational acceleration, 9.8 m s^{-2}. Despite the two different spatial dimensions of the regions sampled by the two instruments, the low-frequency results are surprisingly similar. For the video data the faster sample rate allows us to investigate an additional high-frequency variability. The separation of the low- and the high-frequency-variability regimes occurs in the vicinity of the dominant wind-wave frequency.

A. Scanning-Laser Glint Counts

Figure 1 shows two ±10° scanning-laser glint-count time series. On scales larger than the dominant wind-wave period, these time series have variances that do not decrease significantly as the sample and time-series durations are increased by an order of magnitude. Figure 1(a) contains 5 min of 1-s samples and Fig. 1(b) contains 50 min of 10-s samples. This statistical self-similarity of the glint-count process, and therefore of the surface-roughness variability, is demonstrated further in Fig. 2, which shows histograms for the two glint-count time series of Fig. 1. Whereas Gaussian statistics predict a variance of Fig. 2(b) that is smaller by a factor of 10 than that for Fig. 2(a), in fact the difference is much smaller, less than a factor of 4. This behavior is consistent in the entire data set, regardless of wind speed, atmospheric stability, or sea state.

As the time-series duration increases, the apparently log-normal histogram shape becomes more and more skewed as the low-probability tail is sampled more completely. Log-normal distributions arise in situations that can be characterized by multiplicative processes, and therefore they often are associated with fractals.[13–15] Another useful interpretation is that log-normal processes arise for tasks whose completion depends on prior completion of many steps.[15] It is reasonable to think of the growth process of fractal ocean waves as such a process, where energy is continuously exchanged between waves of different scales. The fact that this implies nonlinear wave–wave interaction over a large range of wavelengths is both interesting and important.

A power spectrum is shown in Fig. 3 for a 75-min average of 2-Hz laser scans taken with $U \approx 5$ m s^{-1} and near-neutral stability. The peak near 0.07 Hz represents swell and corresponds well to the 12–15-s swell periods measured by a collocated downward-looking sonar system. The strength of the swell peak varies throughout our data, but Fig. 3 is reasonably typical. Zosimov and Naugolnykh's[12] power spectra show no obvious swell features, and their personal recollection is of calm seas.[17] The fact that our power spectra do exhibit a swell peak suggests the important possibility that information about swell modulation of short waves is contained in these simple glint counts. An important consequence of this is

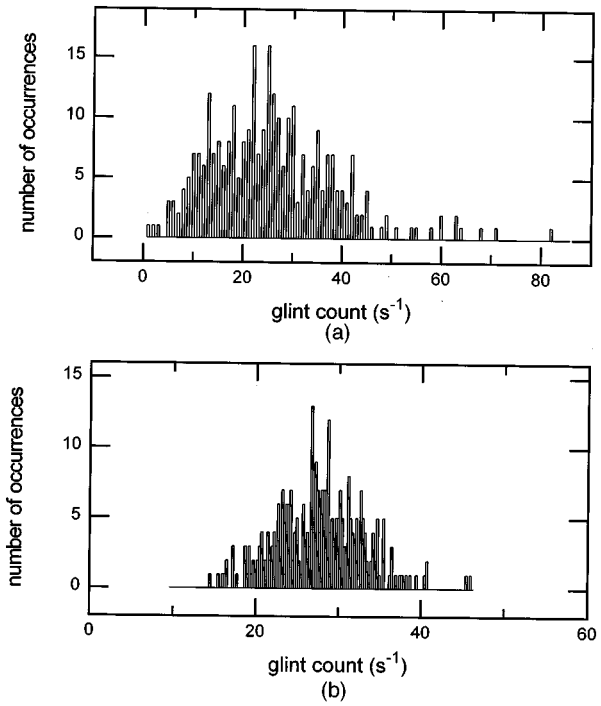

Fig. 2. Glint-count histograms for the time series in Fig. 1. With an order-of-magnitude increase of sample and time-series durations, the histogram width decreased by less than a factor of 2.

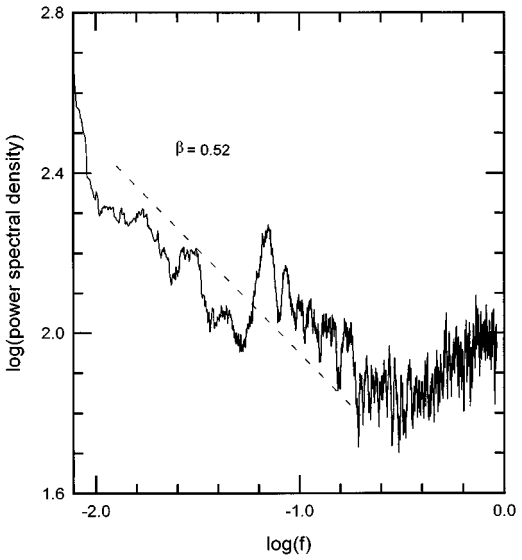

Fig. 3. Typical scanning-laser glint-count power spectrum computed from a 75-min time series of 2-Hz samples ($U \approx 5$ m s^{-1}, 2–3 m swell). The slope chosen for the low-frequency region is indicated by a dashed line segment.

that measurement of the full slope probability-density function or mean square slope may not be necessary for studying long-wave modulation of short waves.

In Fig. 3 an $f^{-\beta}$ type of spectrum exists between approximately 0.01 and 0.20 Hz. The value of the slope exponent β chosen for this particular spectrum is 0.52, shown in Fig. 3 by a dashed line. The mean value of β for the full data set is 0.56 ± 0.05. This is close to Zaslavskii and Sharkov's result[11] of 0.5 and is slightly smaller than Zosimov and Naugolnykh's result of 0.86 for approximately the same frequency range.[12] Also similar to the results of Zosimov and Naugolnykh, our power spectra tend to continue increasing at scales even longer than 100 s. Such behavior and the $f^{-\beta}$ spectral density both suggest surface-roughness variability over scales much larger than the wind-wave correlation length.

The existence of an $f^{-\beta}$ type of power spectrum itself implies a self-similar process, since such a spectrum is inherently scale invariant (i.e., its form is unchanged by multiplicative scaling). Thus these types of spectrum are common and are usually associated with fractal processes having log-normal distributions.[2,3,13–15] According to Eq. (1), time series for our scanning-laser data produce a fractal dimension of the low-frequency glint-count process of 2.22 ± 0.11. This fractal dimension of 2.22 implies a highly wiggly curve for the scanning-laser time series, significantly less random than white noise ($D = 2.5$) but more random than a pure $1/f$ process ($D = 2.0$). Zosimov and Naugolnykh's result[12] of $D = 2.05$ ($\beta = 0.86$), while similar to ours, is closer to a pure $1/f$ behavior, and Zaslavskii and Sharkov's result[11] of $D = 2.25$ ($\beta = 0.5$) is statistically equal to ours.

B. Video-Laser Glint Counts

A similar behavior is found in the video-laser glint counts. As with the scanning-laser data, the histogram variances decrease by no more than a factor of 2 for an order-of-magnitude increase of sample and time-series durations. Because of the video data's higher temporal density, the log-normal histogram shape becomes apparent more rapidly than it does for the scanning-laser data. However, the log-normal distributions from both instruments are similar for an equal number of data points.

Figure 4 shows a glint-count histogram for 5 min of 30-Hz video, which is representative of the histograms we see in data from both instruments for long time averages. The best-fit log-normal function for glint count n_g, shown as a solid curve in Fig. 4, is given by

$$p_g = \frac{4500}{\sqrt{2\pi(1.20)}n_g} \exp\left\{-\frac{[\ln(n_g) - 4.73]^2}{2(1.20)}\right\}. \quad (3)$$

We used a chi-square test to determine the significance of the hypothesis that the histogram in Fig. 4 is indeed given by the log normal in Eq. (3). With the full set of 9000 points, the chi-square test is extremely stringent because of the low level of statistical variability. Indeed, the result of such a test is that we can accept the log-normal hypothesis at only the 10^{-6} level of significance. This low significance may be because of the low-frequency components in the time series that are not treated adequately by the chi-square test as it was applied. A less stringent test can be performed by resampling the same time series at every tenth point and then applying the chi-square test. The result of this test is that we can accept the log-normal hypothesis at the 0.63 level of significance. We conclude that the glint-count histograms are very nearly, although not precisely, log normal. We do not expect precisely log-normal histograms because of very-low-frequency fluctuations in the time series, which are equivalent to nonstationarities over the measurement time.

The video glint-count power spectra differ from the scanning-laser glint power spectra in two notable ways: First, the higher video sampling rate extends the video

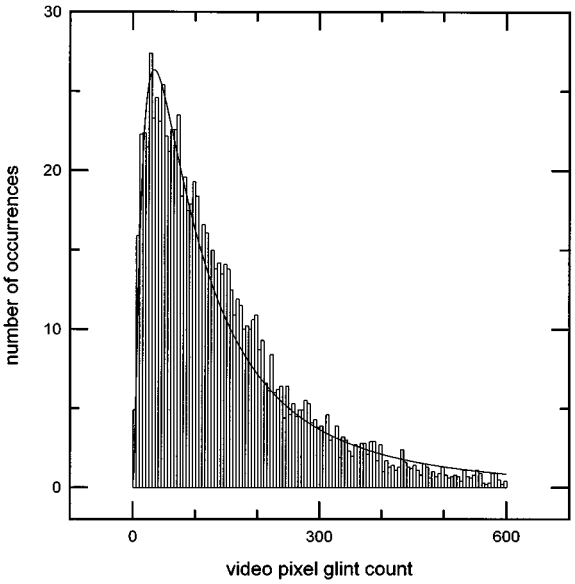

Fig. 4. Video glint count histogram (glint counts from 9000 30-Hz video frames) and the corresponding best-fit log-normal function.

spectrum to higher frequencies; second, the video power spectra tend to roll off instead of continuing to increase in magnitude at the lowest frequencies (below ~0.001 Hz). This second difference may not be significant, though, since the extremely low-frequency tails can be affected by slow changes in the electronics, and they indeed seem to rise less rapidly for shorter scanning-laser time averages. As shown in Fig. 5 for a typical low-wind-speed ($U \approx 1$ m s^{-1}) video glint-count power spectrum, the same type of $f^{-\beta}$ behavior that we found in the scanning-laser spectra exists over a similar frequency range (≈0.01–0.3 Hz), and an additional region with obvious $f^{-\beta}$ form is also evident in the higher-frequency region of approximately 1.5–15 Hz. The values for slope exponents β that we have chosen for the two spectral regions are shown in Fig. 5 with offset dashed lines. The low-frequency slope describes a process involving variability on scales comparable to gravity waves that are longer than the dominant wind wave, and the high-frequency slope describes a process involving variability on scales comparable to wind waves that are shorter than the dominant wind wave.

Wind-speed fluctuations between 1.5 and 3 m s^{-1} also are indicated clearly in the power spectrum of Fig. 5. The feature covering the range of approximately 0.5–1.1 Hz contains multiple peaks that correspond to dominant wind waves for wind speeds at several values in that range. Only a small swell feature is apparent in Fig. 5, for which our log book indicates the presence of 1–1.5-m swell. Video glint power spectra at other times contain more obvious swell peaks near 0.07 Hz. These data contain a combination of much higher wind speeds (≈6 m s^{-1}) and larger swell (≈2–3 m), which is unfortunate for separating out the two effects.

The video glint-count results are surprisingly similar for both pixel and blob counting, which is yet another manifestation of glint-count self-similarity. Figure 6 is a scatter plot that compares the spectral exponents derived by pixel and blob counting. The crosses indicate low-frequency (0.01–0.3 Hz) spectral exponents, and the circles represent high-frequency (1.5–15 Hz) spectral exponents.

There are two distinct clusters of high-frequency exponents and two less-distinct clusters of low-frequency exponents in Fig. 6. This appears to be evidence of stability or wind-speed dependence. The measurements in the smaller-exponent clusters have the highest wind speeds (~6 m s^{-1}) and also have the strongest negative stability of all the measurements. For those three points the air–sea temperature difference was −2.5 °C, whereas for the other measurements it was between +3.2 °C and −0.6 °C. The stability is apparently the most significant factor here for two reasons: (1) Such strong negative stability increases the surface roughness by more than a factor of 2 over the neutral-stability roughness at the same wind speed[16] and (2) other measurements, with 5-m s^{-1} wind speeds but near-neutral stability, produced exponents very close (although at the smaller end) to the higher cluster of data points. The fractal dimensions, calculated from Eq. (1), are summarized in Table 1 for the different cases of low- and high-frequency exponents with strongly negative and near-neutral-to-positive stability.

It seems reasonable for the spectral-exponent magnitudes to become smaller with increasing surface roughness (which occurs for both higher wind speeds and increasingly negative stability), because smaller exponents denote an increasingly random process. In the limit of a zero-value spectral exponent, the process is purely random white noise. Visually, the glint video records at the highest wind speeds are dramatically more random, with much weaker glints than the highly organized patterns

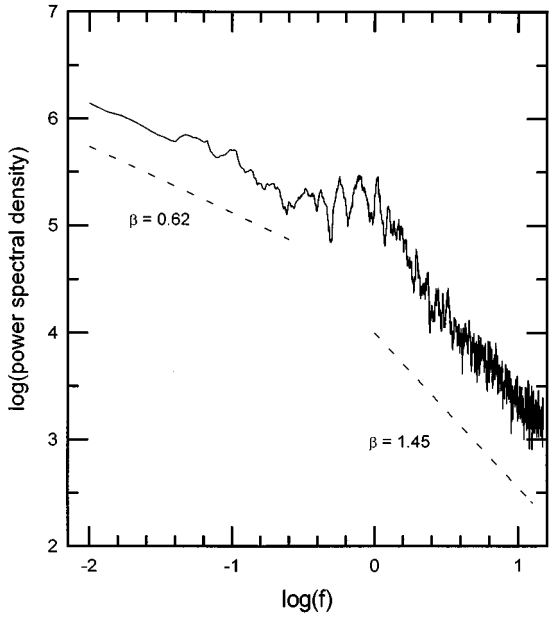

Fig. 5. Video glint-count power spectrum for a 5-min time series of 30-Hz samples ($U \approx 1$ m s^{-1}, 1–1.5 m swell). The intersection of the low- and high-frequency regions occurs at the dominant wind-wave frequency. Dashed-line segments indicate the slopes chosen for these two regions.

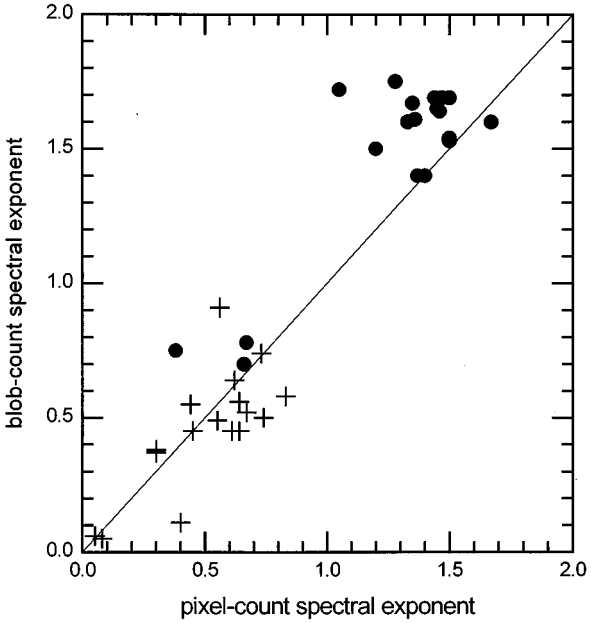

Fig. 6. Scatter plot of spectral exponents for blob and pixel counting. Crosses represent low-frequency exponents; circles represent high-frequency exponents. The exponents become smaller with a rougher ocean surface (see text).

Table 1. Summary of Glint-Count Fractal Dimensions

				Low-Frequency Dimension	High-Frequency Dimension
Scanning Laser				2.22 ± 0.11	NA[a]
Video pixels:	stability	≪	0	2.43 ± 0.07	2.21 ± 0.08
Video pixels:	stability	≳	0	2.20 ± 0.07	1.80 ± 0.07
Video blobs:	stability	≪	0	2.42 ± 0.09	2.13 ± 0.02
Video blobs:	stability	≳	0	2.25 ± 0.10	1.70 ± 0.05

[a] NA, not available.

that appear at the lowest wind speeds. At wind speeds near 1 m s^{-1}, for example, the glint patterns form clearly visible and very bright loops that slowly open and close in rather mesmerizing fashion. Such patterns have been described by Longuet-Higgins,[18] Minnaert,[19] and Lynch and Livingston.[20]

4. DISCUSSION AND CONCLUSIONS

Laser glints from ocean waves form a fractal process in a robust fashion that allows repeatable detection with a variety of measurement techniques. The fractal evidence found along the trail of laser glint time-series analysis provides new ways of thinking about and modeling the glint process and hence surface roughness. For example, if a reliable connection can be found between the fractal dimension and useful physical observables such as wind speed or stability, this type of simple glint counting could be used to provide useful new data from compact and robust instruments. Furthermore, a fractal surface model possibly could provide the geometric input to a finite-difference or moment-method model for computing electromagnetic wave interactions with a realistically rough ocean surface. Repeating such calculations while systematically varying the input variables could yield valuable new insight into radar scattering, microwave polarimetric emission, and other ocean-sensing techniques.

We can compare the glint fractal dimension with the fractal dimension of surface height and slopes by using data from a collocated, downward-looking sonar mounted on the side of the optics module during the experiment. Power spectra of the surface heights during these measurement times follow the theoretical f^{-3} surface-height spectral model extremely well at frequencies above the dominant wind wave (typically ~0.16 Hz). This is essentially the same frequency range as the high-frequency glint variability that we have already discussed. Surface-slope spectra should have an f^{-2} form (by differentiating the height) in the short-wave region. Thus the high-frequency fractal dimension is approximately 1.0 for surface-height time series and 1.5 for surface-slope time series. The glint-count high-frequency fractal dimensions for neutral and positive stability are 1.7 and 1.8 for blobs and pixels, respectively. The similarity of the glint-count and surface-slope fractal dimensions is interesting because, although glints are related to slopes, we do not expect glint-count spectra to be exactly the same as slope spectra.

In this paper we have verified that the fractal behavior of the glint-count process, first pointed out by Zosimov and Naugolnykh,[11] appears to be quite general. The low-frequency variability of glints, and hence surface roughness, beyond the correlation scale of the dominant wind waves suggests that traditional slope statistics may not be entirely sufficient for understanding sea-surface roughness. The additional evidence of long-wave modulation and nonlinear wave–wave interaction that exists in the glint-count histograms and power spectra provides further practical motivation for pursuing this topic. In the video data we have identified a similar high-frequency fractal process at scales smaller than the dominant wind wave. For both scale ranges, but more so for high-frequency variability, the glint-count fractal dimensions appear to be sensitive to stability and wind speed.

ACKNOWLEDGMENTS

We express appreciation to Konstantin Naugolnykh of the National Oceanic and Atmospheric Administration (NOAA)/University of Colorado Cooperative Institute for Research in Environmental Sciences (CIRES) for many illuminating discussions and helpful suggestions, to Michael Falls of NOAA Environmental Technology Laboratory for assistance with the video data processing, and to the FLIP crew for their help with the instrument deployment. This document was prepared as part of a joint NOAA-DoD Advanced Sensors Application Program.

REFERENCES

1. B. B. Mandelbrot, *The Fractal Geometry of Nature* (Freeman, New York, 1983).
2. J. Feder, *Fractals* (Plenum, New York, 1988).
3. M. Schroeder, *Fractals, Chaos, Power Laws: Minutes From an Infinite Paradise* (Freeman, New York, 1991).
4. S. Elgar and G. Mayer-Kress, "Observations of the fractal dimension of deep- and shallow-water ocean surface gravity waves," Physica D **37**, 104–108 (1989).
5. J. Leung and T. Lo, "Chaotic radar signal-processing over the sea," IEEE Trans. Ocean. Eng. **18**, 287–295 (1993).
6. A. J. Palmer, R. A. Kropfli, and C. W. Fairall, "Signatures of deterministic chaos in radar sea clutter and ocean surface winds," CHAOS **5**, 613–616 (1995).
7. M. Stiassnie Y. Agnon, and L. Shemer, "Fractal dimensions of random water surfaces," Physica D **47**, 341–352 (1991).
8. Y. Agnon and M. Stiassnie, "Remote sensing of the roughness of a fractal sea surface," J. Geophys. Res. **96**(C7), 12773–12779 (1991).
9. V. Y. Raizer, V. M. Novikov, and T. Y. Bocharova, "The geometrical and fractal properties of visible radiances associated with breaking waves in the ocean," Ann. Geophysicae **12**, 1229–1233 (1994).
10. V. Y. Rayzer and V. M. Novikov, "Fractal structure of breaking zones for surface waves in the ocean," Izv. Acad. Sci. USSR, Atmos. Oceanic Phys. **26**, 491–494 (1990).
11. G. M. Zaslavskii and E. A. Sharkov, "Fractal properties of breaking zones of sea surface waves," Sov. Phys. Dokl. **32**, 499–501 (1987).
12. V. V. Zosimov and K. A. Naugolnykh, "Fractal structure of large-scale variability of wind-driven waves according to laser-scanning data," CHAOS **4**, 21–24 (1994).
13. B. J. West, "Sensing scaled scintillations," J. Opt. Soc. Am. A **7**, 1074–1100 (1990).

14. B. J. West and M. F. Shlesinger, "On the ubiquity of 1/*f* noise," Int. J. Mod. Phys. B **3**, 795–820 (1989).
15. E. W. Montroll and M. F. Shlesinger, "On 1/*f* noise and distributions with long tails," Proc. Natl. Acad. Sci. USA **79**, 3380–3387 (1982).
16. J. A. Shaw and J. H. Churnside, "Ocean ripple statistics measured with a scanning-laser glint sensor," in *Proceedings of the International Geoscience and Remote Sensing Symposium '96* (Institute of Electrical and Electronics Engineers, New York, 1996), pp. 1328–1330.
17. K. Naugolnykh, NOAA/ETL/ET1, 325 Broadway, Boulder, Colorado 80303 (personal communication, June 1996).
18. M. S. Longuet-Higgins, "Reflection and refraction at a random moving surface. I. Pattern and paths of specular points," J. Opt. Soc. Am. **50**, 838–844 (1960).
19. M. M. Minnaert, *Light and Color in the Open Air* (Dover, New York, 1954).
20. D. K. Lynch and W. Livingston, *Color and Light in Nature* (Cambridge U. Press, Cambridge, 1995), pp. 76–79.